ORIGINAL PAPER

Alireza Salehi · Saeed Mortazavi ⓘ · Mohamadamin Amini

A numerical study of heat transfer in saturated nucleate pool boiling process: a new analysis based on the inherent physics

Abstract In this paper, a direct numerical simulation of saturated nucleate pool boiling is performed using a hybrid front tracking method. A one-field formulation is applied to resolve the mass, momentum and energy equations including phase change. The well-known 1D Estefan problem and 2D film boiling process are studied to validate the implementation of the code. The obtained results are found to be in excellent agreement with the available analytical, numerical and experimental solutions in the literature. Afterward, the developed solver is employed to analyze the nucleate pool boiling problem. The continuous and complete cycles of the nucleate boiling phenomenon involving the corresponding sub-processes are well captured. Unlike the available results in the literature being mostly limited to some common fluids, here the respective non-dimensional parameters are employed to generalize the numerical study findings regardless of the fluid material. The time- and space-averaged Nusselt numbers are considered as a proper criterion to evaluate the heat transfer performance of boiling surface. The main non-dimensional parameters including Grashof, Prandtl and Jacob numbers are varied in the range of 17–300 and 2.8–8.6 as well as 0.017–0.5, respectively. It is observed that any change can cause a frequency variation of bubble departures and the temporal peaks of the space-averaged Nusselt number. Depending on the flow parameters, it is found that the time-averaged Nusselt number experiences an increase or decrease with respect to other cases. Also, the results obtained for nucleate pool boiling simulations show acceptable agreement with the ones predicted by empirical correlations.

List of symbol

c	Specific heat capacity
D_d	Bubble departure diameter
D_{Fritz}	Fritz's bubble departure diameter
g	Acceleration due to gravity
Gr	Grashof number
h_{fg}	Evaporation latent heat
I	Indicator function
Ja	Jacob number
k	Thermal conductivity
L	Distance between two nucleation sites

A. Salehi · S. Mortazavi (✉) · M. Amini
Department of Mechanical Engineering, Isfahan University of Technology, 84156-83111 Isfahan, Iran
e-mail: saeedm@iut.ac.ir

A. Salehi
e-mail: alirezasalehi.mechanic86@gmail.com

M. Amini
e-mail: aminiamin465@gmail.com

l_0	Capillary length
m	Evaporated liquid
N_{pn}	Number of nucleation sites
Nu	Nusselt number
$<Nu>$	Space averaged Nu
$<\overline{Nu}>$	Time and space averaged Nu
P	Pressure
Pr	Prandtl number
q	Heat flux
Re	Reynolds number
T	Temperature
t	Time
u	Velocity vector
U_0	Capillary velocity
x	Position vector

Greek symbols

α	Thermal diffusivity
δ	Delta function
Δ	Normal probe length
$\Delta\tau$	Time step
ϕ	Fluid property
κ	Curvature
μ	Kinetic viscosity of fluid
θ	Contact angle
ρ	Fluid density
σ	Surface tension
τ	Shear stress

Subscripts

crit	Critical
Cycle	Averaged in a cycle
f	Front (interface)
l	Liquid
n	Unit normal vector
sat	Saturation
v	Vapor

Superscripts

$n+1$	Next time step
n	Current time step
*	Dimensionless
.	Time rate

1 Introduction

Multiphase flows with phase change play a fundamental role in natural and industrial processes [1]. Predicting this phenomenon and recognizing its respective features are essential in industrial processes that include multiphase flows and heat transfer. Boiling flows are one of the most important examples having a wide range of applications in many fields of engineering such as power plants, petroleum engineering, design and building

compact and multifunctional heat exchangers, and also in thermal management of electronic cooling. Despite the numerous efforts, nowadays, research on boiling phenomena is a subject of continuing interest [2].

Depending on the presence of the bulk fluid motion, boiling flows are divided in two types, namely flow boiling and pool boiling. In flow boiling, the combination of forced and buoyancy-driven flows provide the fluid motion mechanism while in case of pool boiling only the buoyancy force carries the bubble and surrounding heated liquid away from the heated surface. According to the fluid bulk temperature, both of boiling types (flow or pool) could be classified as subcooled or saturated. The process is known as subcooled or local boiling, if the temperature of the bulk fluid is below the saturation temperature corresponding to system pressure, and saturated or bulk if the temperature of the bulk fluid is equal to saturation temperature. Particularly, in subcooled pool boiling regime the released bubble condenses as it rises across the subcooled liquid, while in saturated pool boiling regime the released bubble could continue its motion up to strike the upper free interface.

Nukiyama [3] was one of the pioneers of studying the boiling phenomenon. He measured heat transfer in pool boiling process from a heated wire for water at atmospheric pressure, experimentally. He noticed that depending on the wall superheat (excess temperature, i.e., Twall-Tsat) various types of pool boiling might occur. The natural convective, nucleate, transient and film boiling were different types of pool boiling regimes that he observed while the wall heat flux was gradually increased.

Nucleate boiling is the most complex process among the other types of pool boiling where the mass, momentum and energy transfer (single- and two-phase) involving a solid wall, liquid and vapor are tightly coupled. The bubble is considered to nucleate when the superheated liquid layer above the site grows sufficiently thick to cause the vapor/gas trapped within the cavity to overcome the surface tension force and grow [4]. As the nucleated bubble starts growing, the buoyancy upward force is also increasing that causes the bubble to overcome the downward surface tension force. At this instant, the bubble departure process within the nucleate pool boiling process will be initiated. So the frequent bubble departure near the boiling surface acts like a pump to displace the bulk liquid and induce a type of free convective currents which will repeat regularly. So there are two mechanisms: the first one is the evaporation of liquid leading to the growth of bubble in the vicinity of the hot heating surface and inside the superheated liquid layer and the second one is induced free convention due to bubble movement. These mechanisms cause heat transfer from the hot boiling surface to bulk liquid during the nucleate pool boiling process.

Among the different pool boiling modes, nucleate boiling has been known as one of the most useful heat transfer in industries like, boilers, heat exchangers, energy storage systems and cooling of electronic components. It is really important for working with equipment in which the boiling process has occurred to know the maximum/critical heat flux in order to avoid the crisis of burnout condition. Burnout condition is a situation that an increase in the boiling surface heat flux leads a sudden and severe increase on amount of wall superheat which will be caused damage on heating surface for exceeded temperature rise. Physically, this happens since the huge amount of nucleation sites cover most part of the boiling surface, so the surrounding liquid could not reach the hot surface through the populated bubble and wet boiling surface. The amount of heat flux, at which the described phenomenon is observed, is well known as critical heat flux. The objective is to design any devices in such a way that they never experience that and should always act in safe side operating condition.

Because of abundant use as well as the complexity of the nucleate boiling process, vast research efforts have been dedicated to this phenomenon over the past decade [5]. With the development of numerical methods for modeling nucleate boiling in recent decades, the numerical study of phase change in liquid/vapor is more helpful.

Generally, in nucleate pool boiling process the heat transfer characteristics are known to be closely associated with nucleation site density of the bubbles attached to the boiling surface. This parameter has been poorly noticed in current numerical/computational works.

Hangjin [6] examined the effect of various surface characteristics including hydrophobic, hydrophilic and heterogeneous wetting surfaces on boiling performance. He found that at low heat fluxes, the hydrophobic surface provides better nucleate boiling heat transfer than the hydrophilic one.

Tien [7] proposed correlations for predicting heat flux on horizontal flat plate at a constant temperature that were in good agreement with experiments at low pressures and heat fluxes. Rohsenow [8] took into account other parameters to obtain heat-flux correlations such as nucleation sites, bubble departure diameter and bubble departure frequency. Their correlations were better at higher pressures. Kocamustafagullari and Ishii [9] presented effective correlations based on the nucleation site density. Further, they suggested better correlation for predicting bubble departure diameter. Sakashita and Kumada [10] improved a correlation for predicting heat flux on a horizontal flat plate. Their correlation was in good agreement with experiments at

high pressures up to 198 bar. Yagov [5] illustrates the different available theoretical approaches to investigate the nucleate pool boiling process. Danish and Mesfer [11] proposed an analytical transient heat conduction model based on the macro-layer near the boiling surface. They found that for higher values of wall superheat, which correspond to nucleate pool boiling; predicted results agree with experimental data.

From the past, most of the studies done in boiling heat transfer have been limited to the experimental works [12] and to obtain semi-experimental correlations based on the relevant curves. With the recent development of computer technology, numerical simulation of boiling turned to be attractive among other methods. One of the first attempts in simulating boiling flows was made by Son and Dhir [13, 14], who studied the evolution of the liquid–vapor interface during saturated film boiling with a level set method. Also, Juric and Tryggvason [15] developed the front tracking method for simulating film boiling on a horizontal surface. Another attempt to simulate boiling, is the study of Li and Kang [16] who simulated pool boiling in nucleate, transient and film boiling phases with lattice Boltzmann (LBM) method. They plotted heat flux versus wall superheat for pool boiling. They also studied the effect of contact angle on nucleate boiling.

There are also other attempts to simulate nucleate boiling. Despite the importance of simulating nucleate boiling, this subject was not taken into consideration until recent years because of its complex behavior and phase change in addition to interface modeling.

Shin and Juric [17] simulated nucleate boiling in three dimensions using a Level Contour Reconstruction method. They placed a hemispherical nucleus at the bottom of the domain as an initial nucleation site. They used a constant wall temperature as the boundary condition of the heated plate and ignored the effect of the heat sink conductivity. They compared the results for the Nusselt number with some experimental correlations. Results for Nusselt number were in good agreement with experimental correlations.

Welch [18] simulated a two-dimensional deformable bubble with moving triangular grids using a semi-implicit finite-volume approach. He calculated bubble growth in nucleate boiling to show the capability of tracking the interface, but could not simulate the full boiling cycle due to inherent limitation of the selected method for manipulating complex topology reconstruction. He could not report the cyclic averaged heat flux for nucleate boiling heat transfer.

Recently, Ryu and Ko [19] simulated nucleate boiling in a two-dimensional domain with lattice Boltzmann method (LBM). They considered constant wall superheat as a boundary condition for the heated surface. They investigated the effect of gravity, Jacob number and contact angle on bubble departure diameter. They validated their results qualitatively with present correlations for the bubble departure diameter which was in good agreement with experimental data. They also studied the effect of nucleation site density on the Nusselt number.

Mohammadpourfard et al. [20] have studied the 2D nucleate pool boiling heat transfer of ferrofluid with water as base fluid, using two-phase and three-phase mixture model. They report that results are in good agreement with experimental ones.

In recent years, Sato and Niceno and their colleagues in Paul Scherrer Institute (PSI) conducted quite extensive works in the field of pool boiling modeling [21], simulation [22] and study the physics of the problem [23]. In summary, they developed a PSI-BOIL code to study the pool boiling problem in different regimes [23] as well as operating condition [24]. The PSI-BOIL is a direct numerical simulation code in which a single set of Navier–Stokes equations is solved under the assumption of an incompressible fluid based on a staggered finite-volume algorithm on Cartesian grids, using an interface tracking method together with a mass-conserving phase change model and a continuum surface force (CSF) model to account the surface tension between different phases. Accordingly, they [22] performed a numerical simulation using PSI-BOIL to model nucleate pool boiling from multiple nucleation sites. Then, the developed method was applied to different pool boiling-water regimes in atmospheric condition, ranging from discrete bubbles to the vapor mushroom region. The imposed thermal boundary condition of the problem was constant heat flux which caused to account the conjugate heat transfer of the boiling surface to obtain the temperature profile. Also, estimation of the nucleation site density and the local activation temperatures are determined from experimental measurement and introduced to the simulation of heterogeneous nucleation where the nucleation only takes place at the interface between the liquid phase and solid phase. They do a comparison of bubble growth and departure shape as well as heat transfer coefficient during the pool boiling with experimental results and observed a good agreement. Santo and Niceno [23] also extended their study to a much general case which included the simulation of pool boiling from nucleate to film boiling region through the critical heat flux.

The complex dynamics of the liquid/vapor interface specially when breaking and coalescence of a departed bubble has occurred, interaction of growing bubble and heating surface, bubble discontinuity across the interface, the unsteady coupling of the mass, momentum and energy equations linked with surface tension, phase

change, and the latent heat effect as well as wall contact angle makes the nucleate boiling process as one of the most difficult problems to investigate in the field of multiphase flows.

This paper will numerically study the nucleate boiling process on a horizontal upwarding flat plate putting in a large pool, where the thermal conductivity and heat capacity of the boiling surface are considered sufficiently large to exclude the effects of fluctuations and distribution of surface temperature on the boiling phenomena [10]. Exerting the constant temperature as boundary condition for the heating surface is a result of this assumption. Also, a periodic boundary condition is employed for side boundaries to include a large pool physics in boiling. The focus of this work is on heterogeneous nucleation in which the interaction of local physics and surface imperfections serve as the primary mechanism for bubble nucleation [25].

The effect of the main non-dimensional parameters on behavior of the heating wall Nusselt number is investigated while the nucleation site density is constant within the isolated bubble region. It is performed by considering the computational domain size and excess temperature of boiling surface corresponding to experimental results of Kocamustafaogullari and Ishii [9]. It should also note that we consider the wall superheat temperature in such a way that the process of the nucleate pool boiling occurs far from the critical heat flux (CHF), all over the present paper. Even if the complete cycle of nucleate boiling including nucleation seed growth, rising and departing from the heated wall is captured, but we focused on overall and mean time averaged of the obtained solution to study the heat transfer during nucleate pool boiling.

According to the best knowledge of the authors, the described research has not been already studied with the current point of view and methodology. The major highlights of this paper are summarized as follows:

(a) For the first time, a hybrid front tracking technique presented by Esmaeeli and Tryggvason [26] is developed and applied in order to simulate saturated nucleate pool boiling process for several sequential cycles.
(b) Using the presented new point of view, regardless of the fluid material, the behavior of the hot wall Nusselt number is studied versus different dimensionless parameters.
(c) Effect of high pressures on nucleate boiling with different fluid properties has been taken into account where any reliable experimental results are not available.
(d) As a complete quasi-steady process, direct numerical simulation of the saturated nucleate pool boiling is well captured including formation, growth, detachment and rising of the departed bubble as well as breaking through the top interface, sequentially.

2 Governing equations and numerical method

2.1 Mathematical formulation

For boiling problems, whether it is pool or flow, the mass, momentum and energy equations are written in conservative form as follows:

$$\frac{\partial \rho}{\partial t} + \nabla \cdot \rho \overline{u} = 0, \tag{1}$$

$$\frac{\partial \rho \overline{u}}{\partial t} + \nabla \cdot \rho \overline{u}\overline{u} = -\nabla p + \rho \overline{g} + \nabla \cdot \mu \left(\nabla \overline{u} + \nabla \overline{u}^T \right) + \overline{f}, \tag{2}$$

$$\left(\frac{\partial \rho c T}{\partial t} + \nabla \cdot \rho c \overline{u} T \right) = \nabla \cdot k \nabla T + g. \tag{3}$$

Note that the viscous dissipation term is neglected in Eq. (3). Although the mentioned equations for boiling flows are applicable inside both phases, the appropriate jump conditions for mass momentum and energy should be implemented at the interface as well:

$$\rho_l(\overline{u_l} - \overline{u_f}) \cdot \overline{n} = \rho_v(\overline{u_v} - \overline{u_f}) \cdot \overline{n} = \dot{m}, \tag{4}$$

$$\dot{m}(\overline{u_v} - \overline{u_l}) = (\tau_v - \tau_l).\overline{n} - (p_v - p_l)I \cdot \overline{n} + \sigma \kappa \overline{n}, \tag{5}$$

$$\dot{m}h_{fg} = \dot{q} = q''_{liquid} - q''_{vapor} = k_v \left. \frac{\partial T}{\partial n} \right|_v - k_l \left. \frac{\partial T}{\partial n} \right|_l. \tag{6}$$

Here, $\overline{u_l}$ and $\overline{u_v}$ are fluid velocities in the liquid and vapor side of the interface, respectively. Also, $\overline{u_f}$ denotes the interface velocity, and $\dot{m}$ represents the evaporation rate of liquid phase at the interface. It is assumed that the interface is at the saturation temperature (T_f) corresponding to the pressure of the boiling system [26].

For implementing a numerical procedure, the so-called single-fluid method, in which one set of the equations is solved for the whole computational domain, is used. In this approach, the governing differential equations are modified such that one can recover the original form inside each phase (Eqs. (1)–(3)) as well as the jump conditions are simultaneously satisfied at the interface. Accordingly, the momentum and the thermal energy equations take the following form:

$$\frac{\partial \rho \overline{u}}{\partial t} + \nabla \cdot \rho \overline{uu} = -\nabla p + \rho \overline{g} + \nabla \cdot \mu \left(\nabla \overline{u} + \nabla \overline{u}^{\mathrm{T}} \right) + \sigma \int \delta(\overline{x} - \overline{x}_{\mathrm{f}}) \kappa_{\mathrm{f}} \overline{n}_{\mathrm{f}} dA_{\mathrm{f}}, \tag{7}$$

$$\left(\frac{\partial \rho c T}{\partial t} + \nabla \cdot \rho c \overline{u} T \right) = \nabla \cdot k \nabla T - \left[1 - (c_{\mathrm{v}} - c_{\mathrm{l}}) \frac{T_{\mathrm{sat}}}{h_{\mathrm{fg}}} \right] \int \delta(\overline{x} - \overline{x}_{\mathrm{f}}) \dot{q}_{\mathrm{f}} dA_{\mathrm{f}}. \tag{8}$$

Here, δ is a two- or three-dimensional delta function constructed by successive multiplication of one-dimensional delta function. Also, $\overline{x}$ represents a position in Eulerian coordinate system, and $\overline{x}_f$ denotes the position of the front. The quantities having the subscript f are evaluated at the front. When there is no phase change (far from the interface), Eq. (1), i.e., the mass conservation, is simplified to $\nabla \cdot \overline{u} = 0$ for incompressible flows. Under this condition, where the conservation of mass is basically divergence free for the velocity field, this equation will be a part of Navier–Stokes equations. Otherwise in the neighborhood of the phase boundary, Eq. (13), which is derived in the following, has to be solved using Eqs. (7) and (8), simultaneously. Actually, incompressibility condition is satisfied throughout both phases except at the interface where the evaporation takes place. According to the algorithm developed by Tryggvason et al. [15], the velocity field can be written as

$$\overline{u} = \overline{u}_{\mathrm{v}} I + \overline{u}_{\mathrm{l}}(1 - I). \tag{9}$$

In Eq. (9), I represents an indicator function (i.e., a Heaviside function) being one and zero in the vapor and liquid phases, respectively. It should be noted that this relation implies that the velocity field in each phase has a smooth incompressible extension into the other one. The gradient of indicator function is zero over the computational domain except at the interface. The gradient of the indicator function can be expressed in terms of the front properties:

$$\nabla I = \int \delta(\overline{x} - \overline{x}_{\mathrm{f}}) \overline{n}_{\mathrm{f}} dA_{\mathrm{f}}. \tag{10}$$

Taking the divergence of Eq. (9), using Eq. (10), and assuming that $\nabla \cdot \overline{u_v} = \nabla \cdot \overline{u_l} = 0$ yields

$$\nabla \cdot u = \int \delta(\overline{x} - \overline{x}_{\mathrm{f}})(\overline{u}_{\mathrm{v}} - \overline{u}_{\mathrm{l}}) \cdot \overline{n}_{\mathrm{f}} dA_{\mathrm{f}}. \tag{11}$$

The difference between the velocity of the liquid and the velocity of the vapor at the interface is associated with the evaporation rate. One can eliminate $\overline{u}_{\mathrm{f}}$ in Eq. (4) and noting that $\dot{m} = \frac{\dot{q}}{h_{\mathrm{fg}}}$, this results in

$$(\overline{u}_{\mathrm{v}} - \overline{u}_{\mathrm{l}}) \cdot \overline{n} = \frac{\dot{q}_{\mathrm{f}}}{h_{\mathrm{fg}}} \left(\frac{1}{\rho_{\mathrm{v}}} - \frac{1}{\rho_{\mathrm{l}}} \right). \tag{12}$$

Inserting the expression for the velocity difference across the interface from Eq. (12) into Eq. (11) results in the modified equation for mass conservation:

$$\nabla \cdot \overline{u} = \frac{1}{h_{\mathrm{fg}}} \left(\frac{1}{\rho_{\mathrm{v}}} - \frac{1}{\rho_{\mathrm{l}}} \right) \int \delta(\overline{x} - \overline{x}_{\mathrm{f}}) \dot{q}_{\mathrm{f}} dA_{\mathrm{f}}. \tag{13}$$

In summary, the governing equations to solve are Eqs. (7), (8) and (13). These equations will be solved by a second-order finite difference/front tracking method on a staggered grid. By using a predictor–corrector approach, the time integration proceeds in two steps.

2.2 Numerical method

The phase boundary is represented by a logical collection of triangular elements in three dimensions and line segments in two dimensions [15, 27]. The elements are interconnected together by a linked-list, that are responsible to transfer data between the stationary grid and the interface grid and are advected by the flow velocity field [28]. The indicator function must be determined at the beginning of each time step. This parameter is computed through Eq. (10). Taking the divergence of this equation results in a Poisson equation for the indicator function:

$$\nabla^2 I = \nabla \cdot \int \delta(\overline{x} - \overline{x_f})\overline{n_f}\mathrm{d}A_f. \tag{14}$$

The right-hand side of Eq. (14) is computed by calculating $\overline{n_f}\mathrm{d}A_f$ for each front element and then distributing it on the stationary grid using a smoothed delta function [29]. This equation can be solved by a fast Poisson solver [30] and the fluid properties $\varphi^n \equiv (\rho^n, \mu^n, k^n, c^n)$ are determined at the current time step using $\varphi^n = \varphi_v I^n + \varphi_l(1 - I^n)$; the superscript n denotes the time index. Next, the velocity and the temperature fields can be evaluated. The heat source $\dot{q}_f$ is determined by applying the method of Udaykumar et al. [31] and computing the right-hand side of Eq. (6) through a first-order finite difference approximation:

$$\dot{q}_f = \frac{1}{\Delta}[k_v(T_v - T_{sat}) - k_l(T_l - T_{sat})], \tag{15}$$

where T_l and T_v are the temperature of the liquid and vapor sides, sufficiently close to the interface at locations $\overline{x_l}$ and the $\overline{x_v}$, respectively. Assuming the liquid–vapor interface temperature is equal to the saturation temperature of the liquid corresponding to the system pressure would be the fundamental physical approximation made here [24]. T_l and T_v are obtained by interpolating the temperature at $\overline{x_l} = \overline{x_f} - \Delta\overline{n_f}$ and $\overline{x_v} = \overline{x_f} + \Delta\overline{n_f}$ using two normal probes originating at the phase boundary and extend a distance Δ into the liquid and the vapor. Here, $\overline{x} = (x, y, z)$ is measured with respect to a fixed coordinate frame. Numerical experiments revealed that the results obtained are insensitive to the length of normal probes as long as $h \le \Delta \le 2h$, where h is the grid spacing. The term $\dot{q}_f$ in Eq. (8) is distributed on to the stationary grid using Peskin distribution [15].

In the proposed method of Juric and Tryggvason [32], the heat source was iteratively evaluated by adjusting it until the interface temperature at the end of each time step was correct. Using the procedure developed by Esmaeeli and Tryggvason [26] removes this iteration. To move the phase boundary, one could simply integrate

$$\frac{\mathrm{d}\overline{x}_f}{\mathrm{d}t} = u_n\overline{n}_f, \tag{16}$$

where $u_n = \overline{u_f} \cdot \overline{n}$. The normal component of the velocity of the interface can be evaluated from Eq. (4) in conjunction with Eq. (6):

$$u_n = \frac{1}{2}(\overline{u}_l + \overline{u}_v) \cdot \overline{n} - \frac{\dot{q}_f}{2h_{fg}}\left(\frac{1}{\rho_v} + \frac{1}{\rho_l}\right). \tag{17}$$

Consequently, as Eq. (17) reveals the interface normal velocity has two terms; the first term is due to the fluid advection and the second term is originated from the phase change. The former is determined by Peskin interpolation method [29] and the latter is evaluated through Eq. (15). The new front position will be given at the next time step through integrating Eq. (16), $\overline{x}_f^{n+1} = \overline{x}_f^n + \Delta t u_n\overline{n}_f$. It should also be pointed out that here in pool boiling process the interface is moved based on the normal velocity projected to the normal to the interface at every point. This is the main difference that differentiate the method from flow boiling. As a result, due to the applied method for the movement of the interface, it is only valid for pool boiling.

Then, from Eq. (14), the indicator function with respect to the new position of the front, I^{n+1} is calculated and the density and the heat capacity fields at the next time step, ρ^{n+1}, c^{n+1}, are calculated, as well. The energy equation in a semi-discretized form could be written as follows:

$$\frac{\rho^{n+1}c^{n+1}T^{n+1} - \rho^n c^n T^n}{\Delta t} = A^n, \tag{18}$$

so that A denotes the right-hand side of Eq. (8) including the advection, the diffusion and the source term. Using the Peskin distribution function, the surface tension is distributed on to the stationary grid. The momentum equation in semi-discretized form is

$$\frac{\rho^{n+1}u^{n+1} - \rho^n u^n}{\Delta t} = -\nabla p + B, \tag{19}$$
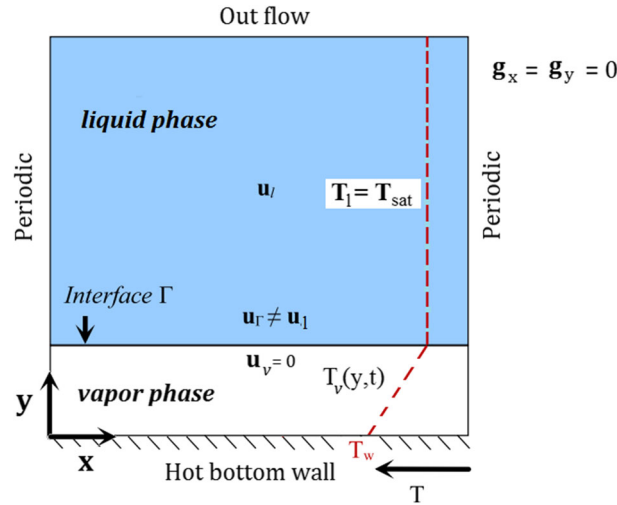
Fig. 1 Schematic layout for 1D Stefan problem

where the advection, diffusion, gravitational body force and surface tension force are represented by *B*.

Close to the surface, two front elements are connected to the wall surface by fixing one of the markers points of these elements on the wall. Thus, these two elements are always attached to the wall. Regarding the contact angle with the wall, no restriction is imposed by the numerical method. The contact angle is just set by the motion of the front and the surface tension force applied by the curvature of the front adjacent to the wall.

3 Results and discussion

Before starting to study the nucleate pool boiling problem, some case studies are accomplished to verify and validate our developed code. We will next focus on some details and overall solution obtained for nucleate pool boiling process under various conditions.

3.1 Validation of phase change model (Stefan problem)

To validate the developed code and in particular determine how the implemented temperature gradient-based phase change model works [18], the so-called Stefan problem [33, 34] is considered in this section. Figure 1 depicts the problem of this study with the applied boundary conditions as well as important parameters, schematically.

Just some illustrations regarding the considered problem and applied boundary conditions are presented as the following. Here, the vapor phase is located near the hot bottom wall and liquid phase is at the top of domain. The bottom boundary is considered as a solid wall with a constant uniform temperature, while an outflow boundary condition is imposed at the top boundary. Furthermore, the periodic boundary conditions are applied to the left and right boundaries to keep the problem essentially one dimensional.

Based on the problem setup, the location of the interface and velocity of the liquid phase are calculated numerically under different flow conditions such as the density ratio. We compare our results with the analytical solutions which are not presented here for the sake of brevity and frequently used in the literature [14, 33, 35]. The liquid and vapor phases are separated by a horizontal interface initially located at the position $y = 0.1$. The bottom wall is heated and the heat transfer to the vapor by diffusion causes liquid evaporation close to interface. Once the evaporation starts the interface moves upward due to excess vapor formed. Consequently, during change of phase the remainder liquid gets a positive velocity and part of it exits from the top boundary.

The dimensions of computational domain is selected as a 1×1 (m^2). The fluid properties, bottom wall temperature as well as the saturation temperature applied here are as follows:

$$\rho_l = 2.5, \rho_v = 0.5, \ \mu_v = 0.007, \ \mu_l = 0.098,$$
$$k_v = 0.0035, \ k_l = 0.0015, c_v = 1.0, c_l = 1.0, \quad (20)$$
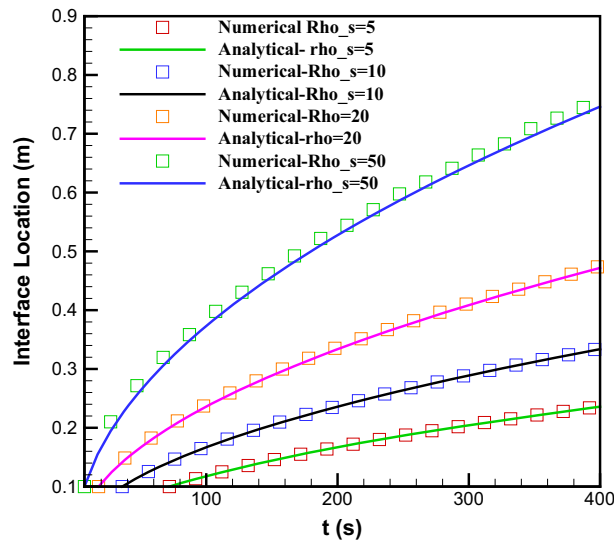$$h_{lv} = 100.0, \ T_w = 12.0, \ T_{sat} = 10.0,$$

Fig. 2 Comparison between the numerical solution and analytical one for the interface location at different density ratios
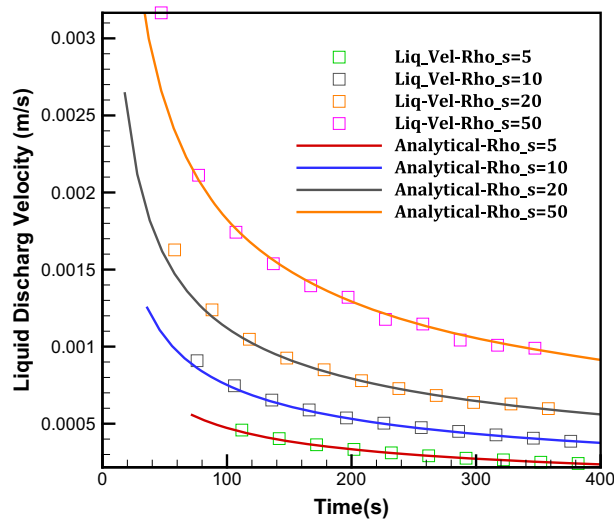

Fig. 3 Comparison of the discharge liquid velocity with analytical solution for Estefan problem at different density ratios

where all of the parameters are in standard SI units. The results obtained for the position of the interface with respect to time are presented in Fig. 2. Simulations are performed at different density ratios.

As shown in Fig. 2, good agreement with analytic solution is observed at different density ratios. The maximum relative error is less than 1% while the computational grid size is still not very fine, i.e., 64×64.

Figure 3 shows the corresponding results for the liquid velocity due to the phase change as a function of time. As it is observed, the discharge velocity of the liquid severely increases as the density ratio is raised. Once again, the results are in good agreement with analytical solution. The described procedure was also repeated in the horizontal direction and the same results were also obtained. So, regardless of the interface orientation in the computational domain, the implemented phase change model works properly.

3.2 Validation of the code (film boiling problem)

The film boiling process is considered as a second benchmark to study and validate the code. The well-defined problem of a single mode of 2D film boiling of water at a high pressure ($P = 0.765 P_{cr}$) which has already
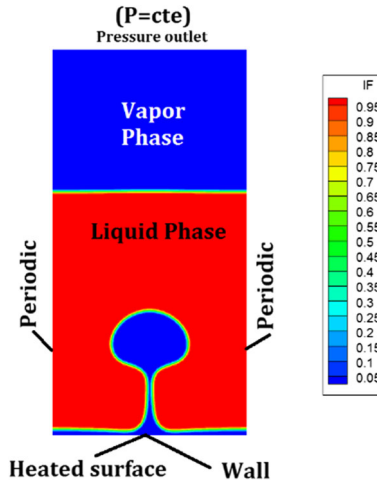
Fig. 4 Computational domain layout, size ($\lambda_{d2} \times 2\lambda_{d2}$), considered to study the film boiling process
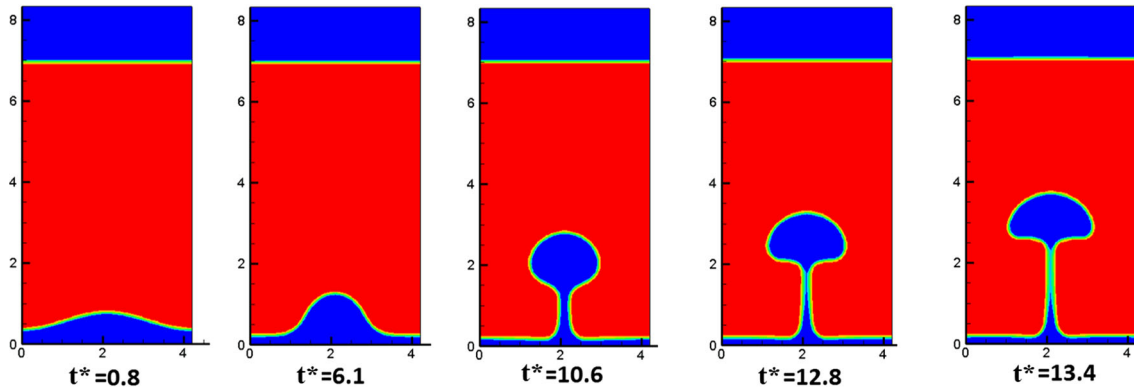

Fig. 5 The time evolution contour plots of phases field from the early instants up to the first breakup of the rising bubble during the film boiling process of water at high pressure ($P = 0.765\ P_{cr}$)

been analyzed by Esmaeeli and Tryggvason [26] is proposed here. The main non-dimensional parameters are listed below:

$$Gr = 17.85, \ Ja = 0.064, \ Pr = 4.2,$$
$$\frac{\rho_v}{\rho_l} = 0.21, \ \frac{\mu_v}{\mu_l} = 0.386, \ \frac{k_v}{k_l} = 0.28, \ \frac{c_v}{c_l} = 1.83. \tag{21}$$

The computational domain, its dimensions as well as implemented boundary conditions are shown in Fig. 4.

The time evolution of liquid/vapor interface according to the phases field contour plot is shown in Fig. 5 where various dimensionless time (t^*) from 0.8 to 13.4 is displayed. It should be noted that a characteristic time is used equal to the capillary length scale divided by characteristic velocity according to Eq. (32). The variation of heating surface space-averaged Nusselt number, <Nu>, versus dimensionless time is plotted in Fig. 6a. As it can be observed at the initial instants (first growth of the initial bubble) the heat transfer rate is significantly high. This is due to the initial temperature distribution which is considered as the saturation temperature corresponding to the system pressure that creates a severe temperature gradient at the beginning of the simulation. If the simulation continues for a longer time some rising bubbles will depart from the bottom vapor layer, repeatedly. This is necessary in order to capture the time where a quasi-steady state is established.

Figure 6b presents the behavior of the space-averaged Nusselt number versus time up to time $t^* = 330$. As it is observed, the quasi-steady state reaches at around time $t^* = 60$. Afterward, the dynamics of the growing, rising and departing bubbles will repeatedly occur for subsequent cycles. Under the considered condition, the time- and space-averaged Nusselt number, $<\overline{Nu}>$, does not depend on initial condition or number of cycles
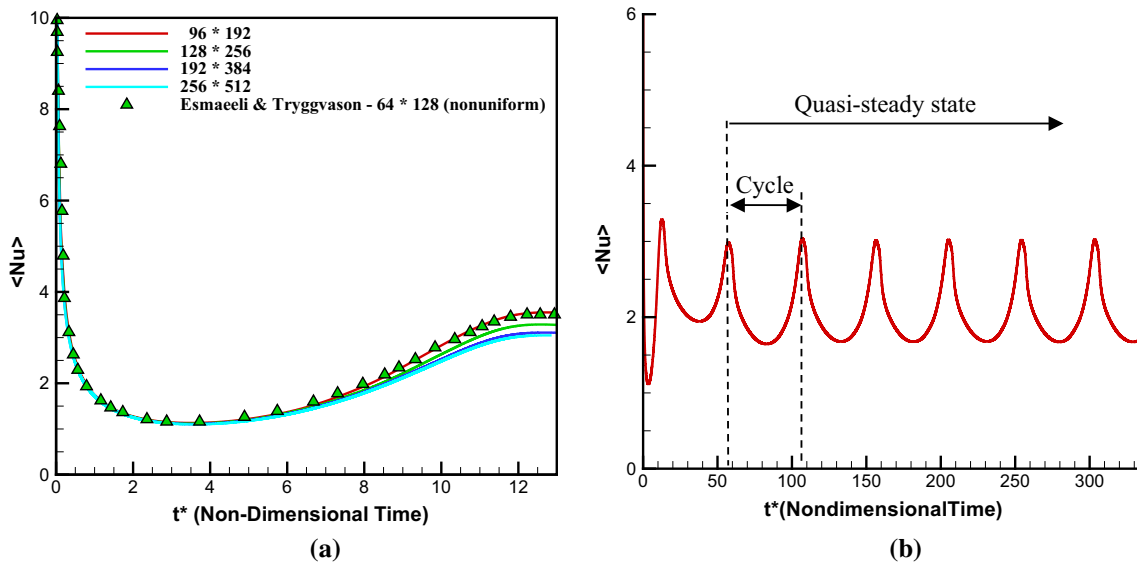
Fig. 6 Space-averaged Nusselt number on the heating plate against dimensionless time: **a** comparison of the present study and those reported by [26, 36] from the initial time to just before the first bubble departure and **b** in case where the simulation proceeds to capture the departure of seven growing bubbles (quasi-steady state)

Table 1 Summary of the result obtained for time- and space-averaged Nusselt number and other experimental and numerical studies—Gr = 17.85, Pr = 4.2, Ja = 0.064

Description	Time- and space-averaged Nusselt number $<\overline{Nu}>$	Relative error %		
		Numerical work	Berenson's correlation	Klimenko's correlation
Present study (numerical simulation)	2.057	1%	+ 17%	− 20%
Esmaeeli and Tryggvason [36] (numerical simulation)	2.08	Ref. value	Not applicable	Not applicable
Berenson's Correlation [37] NuBerenson = 0.425 (Gr × Pr/Ja)0.25	2.48	Not applicable	Ref. value	Not applicable
Klimenko's correlation [38] NuL-Klimenko = 0.169 (Gr × Pr/Ja)(1/3)	1.78	Not applicable	Not applicable	Ref. value

in which the simulation has proceeded. The time- and space-averaged Nusselt number is compared with other numerical efforts and experimental correlations in Table 1.

The result obtained shows an excellent agreement with those reported by Esmaeeli and Tryggvason [26, 36]. Also, our simulation results lie between the ones determined by Klimenko and Berenson correlations. As it is discussed by Esmaeili and Tryggvason [5], the good agreement with experimentally observed heat transfer rates for two-dimensional system suggests that a 2D simulations capture much of the dynamics.

3.3 Problem setup and computational domain description

Laminar and unsteady two-phase flow with phase change is simulated using a front tracking method. The phase change process and the respective mass transfer are allowed to occur across the interface. Both the vapor and liquid phases are incompressible and the compressibility effects due to phase change only exist across the phase boundary. As shown in Fig. 7, all simulations are carried out in a 2D planar domain. Initially, a semicircle vapor bubble is placed on a horizontal surface as an initial seed for the specified nucleation site density.

Initially, both the vapor and liquid are at saturation temperature corresponding to system pressure. An upper interface located initially at $y = 5.2$ is considered in order to have more realistic behavior of the rising
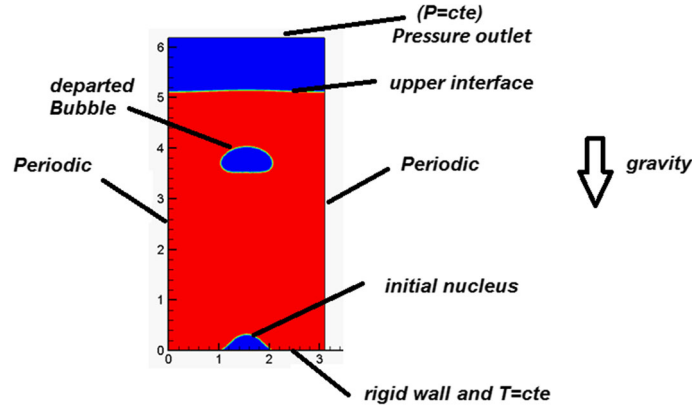
Fig. 7 Computational domain and respective boundary conditions ($\lambda_{d2} \times 2\lambda_{d2}$) for two-dimensional nucleate boiling

bubble. So the departed bubble will break through the top vapor layer and the bubble growth and departure cycles are repeated this way.

A periodic boundary condition is applied for lateral boundaries to implement a large pool condition. Non-slip boundary condition is applied to the heated surface having constant excess temperature ($T_w > T_{sat}$). Also, the pressure outlet boundary condition is selected for the top boundary. The size of initial nucleation site is chosen equal to bubble departure diameter that is reported by Kocamustafaogullari and Ishii [9] as follows:

$$D_d = 0.0012 \left(\frac{\rho_l - \rho_v}{\rho_v} \right)^{0.9} (D_{Fritz}), \tag{22}$$

where D_{Fritz} is defined as

$$D_{Fritz} = 0.0208\theta \sqrt{\frac{\sigma}{g(\rho_l - \rho_v)}}, \tag{23}$$

where θ is the contact angle that is measured in degrees. The geometrical contact angle is imposed to be 90° for all simulations. The diameter of initial seed bubble is taken as 1.0 in the present study.

Kocamustafaogullari and Ishii [9] also reported a correlation between wall superheat and nucleation site density, N_{pn}, for water boiling at pressures up to 198 atmospheres:

$$N_{pn} = \frac{N_{pn}^*}{D_d^2}, \tag{24}$$

where N_{pn}^* is defined as follows:

$$N_{pn}^* = f \left(\frac{\rho_l - \rho_v}{\rho_v} \right) R_c^{*-4.4}, \tag{25}$$

where R_c^* and $f \left(\frac{\rho_l - \rho_v}{\rho_v} \right)$ are:

$$R_c^* = \frac{R_c}{D_d/2}, \tag{26}$$

$$f \left(\frac{\rho_l - \rho_v}{\rho_v} \right) = 2.157 \times 10^{-7} \left(\frac{\rho_l - \rho_v}{\rho_v} \right)^{-3.2} \left(1 + 0.0049 \left(\frac{\rho_l - \rho_v}{\rho_v} \right) \right)^{4.13}, \tag{27}$$

where R_c is defined as

$$R_c = \frac{2\sigma \left[1 + (\rho_v/\rho_l) \right] / P}{\exp \left[h_{fg} \Delta T_{sat} / (R T_w T_{sat}) \right] - 1}, \tag{28}$$

Table 2 Properties ratios of water at $p_{\text{sat}} = 170$ bara

ρ^*	c^*	κ^*	μ^*	Gr	Pr
0.21	1.83	0.28	0.386	78×104	4.2

Table 3 Capillary length, characteristic velocity and computational domain size

l_0	U_0	$L_x^* \times L_y^*$
0.2571	0.717	3.1×6.2

and L is defined as

$$L = \frac{1.0}{\sqrt{N_{pn}}}. \tag{29}$$

Here, L is the average distance between two nucleation sites. In the present study, the box size is chosen to be L^*, as a non-dimensional box size, defined as:

$$L_x^* = \frac{L}{D_d}. \tag{30}$$

3.4 Governing dimensionless parameters

The pertinent dimensionless parameters for this study are Grashof (Gr), Jacob (Ja) and Prandtl (Pr) numbers as well as ratio of liquid/vapor properties that are defined as follows:

$$
\begin{aligned}
&\rho^* = \frac{\rho_v}{\rho_l} && k^* = \frac{k_v}{k_l} \\
&\mu^* = \frac{\mu_v}{\mu_l} && c^* = \frac{c_v}{c_l} \\
&\text{Gr} = \frac{\rho_v(\rho_l - \rho_v)gl_0^3}{\mu_v^2} && \text{Ja} = \frac{c_v(T_w - T_{\text{sat}})}{h_{fg}} \\
&\text{Pr} = \frac{\mu_v c_v}{k_v} && \text{Nu} = -\frac{l_0}{(T_w - T_{\text{sat}})} \frac{\partial T}{\partial y}\Big|_{y=0}
\end{aligned}
\tag{31}
$$

where l_0, U_0, and t_0. are defined as characteristics length, velocity and time, respectively:

$$
\begin{aligned}
l_0 &= \sqrt{\frac{\sigma}{g(\rho_l - \rho_v)}}, \\
U_0 &= \sqrt{l_0 g}, \\
t_0 &= \sqrt{\frac{l_0}{g}}.
\end{aligned}
\tag{32}
$$

As presented in Table 2, the thermo-physical property ratios used here are the same as those of saturated water at $P_{\text{sat}} = 170$ (bara), except for Grashof number, which will change in the range of 18–300 in the present numerical investigation [36]. The smaller Grashof number is implemented in the problem by considering the gravitational acceleration greater than its usual value or considering a more viscous fluid.

Also, capillary length, velocity scale and box size are those that are tabulated in Table 3. The box size in the lateral direction has been taken large enough so that the bubble departure will definitely take place.

In the following, the effects of dimensionless parameters including Grashof, Prandtl and Jacob will be studied in detail at a constant nucleation site density and a fixed properties ratio. To better understand the effect of each dimensionless number, the remaining non-dimensional parameters are fixed during the study.

3.5 Grid independence of the solution

Different grid resolutions are examined to ensure that the simulation results for nucleate pool boiling are independent with respect to the computational grid. The space-averaged Nusselt as well as the first bubble departure time are selected as two different proper criteria for grid independence of the solution. The summery of the results obtained are presented in Fig. 8. The performed grid study is done under the condition of $Gr = 300$, $Pr = 4.2$ and $Ja = 0.017$. According to results obtained the time varying Nusselt numbers are quite similar for fine grid resolutions. It should be pointed out the space-averaged Nusselt number is directly related to the temperature gradient at the heating surface which is very sensitive to the grid spacing adjacent to the wall. Figure 8a shows the space-averaged Nu versus time up to the time where the first bubble has departed for different grid resolutions. Comparison of results reveals that the space-averaged Nusselt number for two last finest grids, i.e., 374×768 and 512×1024, are quite close. Figure 8b shows the exact time for the first bubble departure for every grid resolution (i.e., grid numbers 1–5). As it can be seen for two finest grid resolutions, a good convergence for bubble departure time is achieved. Also the corresponding front position at various grid resolutions is presented in Fig. 8c with details. As it can be observed, the front location for two fine grid resolutions is nearly the same. Accordingly, the 374×768 grid resolution is quite reasonable to capture the flow details. As a result, this grid resolution has been chosen to report the rest of simulation results.

The initial transient time is relatively short in comparison with the total time of the simulation where the time- and space-averaged Nusselt number results are reported. Also, regarding the breakup and coalescence it should be noted that these phenomena directly occur on molecular scale, however we try to model and study them in a continuum scale. Although the inherent physics of the break off and coalescence of the bubbles are still under investigation using numerical tools [39, 40], here, the topology change is simply done whenever the thickness of the thin thread is smaller than two grid spacing [34]. The developed procedure and other details in the level of code implementation using front tracking solver are presented by Razizadeh et al.[41]. Although changing this criteria might affect the results a little bit or temporary, the overall averaged or statistical results will remain essentially the same [40, 41]. Once a bubble is departed from the bottom vapor layer then the severe local surface tension will pull down the remaining vapor layer and the process is repeated over time. The described phenomena is well known as the rewetting which is one of the nucleate pool boiling sub-processes.

The developed code is tested in case of a continuous breaking off and coalescence during a few complete cycles where the results are shown in Fig. 9. Here, we examine the case of a high Jacob number where several bubbles generate during a relatively short time interval. The space- and time-averaged Nusselt number are computed in two different ways. As it is specified in Fig. 9, the first choice is for the whole simulation time in the range of [0–320] and the second is for one cycle only in the range of [50–80]. The former Nusselt number is equal to $<\overline{Nu}> = 1.283$ as it is also plotted by a straight line in the figure and the latter is equal to $<\overline{Nu}> = 1.282$.

As these values are very close to each other, it is concluded that the initial condition and starting time have really insignificant effect on the overall result. Also, under the considered condition (Long enough time for simulation) the corresponding result for just one cycle is nearly the same as the whole time of simulation. Accordingly, we consider the time interval of the third cycle right after the second departure as a corresponding time integration interval to report the space- and time-averaged Nusselt number, $<\overline{Nu}>$, for the rest of the simulations as well.

3.6 Validating nucleate boiling results using experimental correlations

Because of complexity and nonlinear behavior of boiling flows [4, 42], not only there is not any analytical solution for nucleate pool boiling problem but also all of the experimental results are limited to a few cases of common fluids usually examined at atmospheric conditions [43] and devoted to specific combination of working fluids and material of the boiling surface [44]. Besides, there are some mechanistic models based on some dominant sub-processes present on the boiling problem and used a couple of closure coefficients inside the correlation as the fitting parameter. Applying these models is very limited and strongly depends on reliable experimental data. These closures usually depend on the working fluid property, boiling surface and geometry as well as system operating pressure [21, 22]. However, it seems that there is still considerable amount of unknown physics involved that includes nonlinear interactions of several sub-processes which need to be clarified [45].
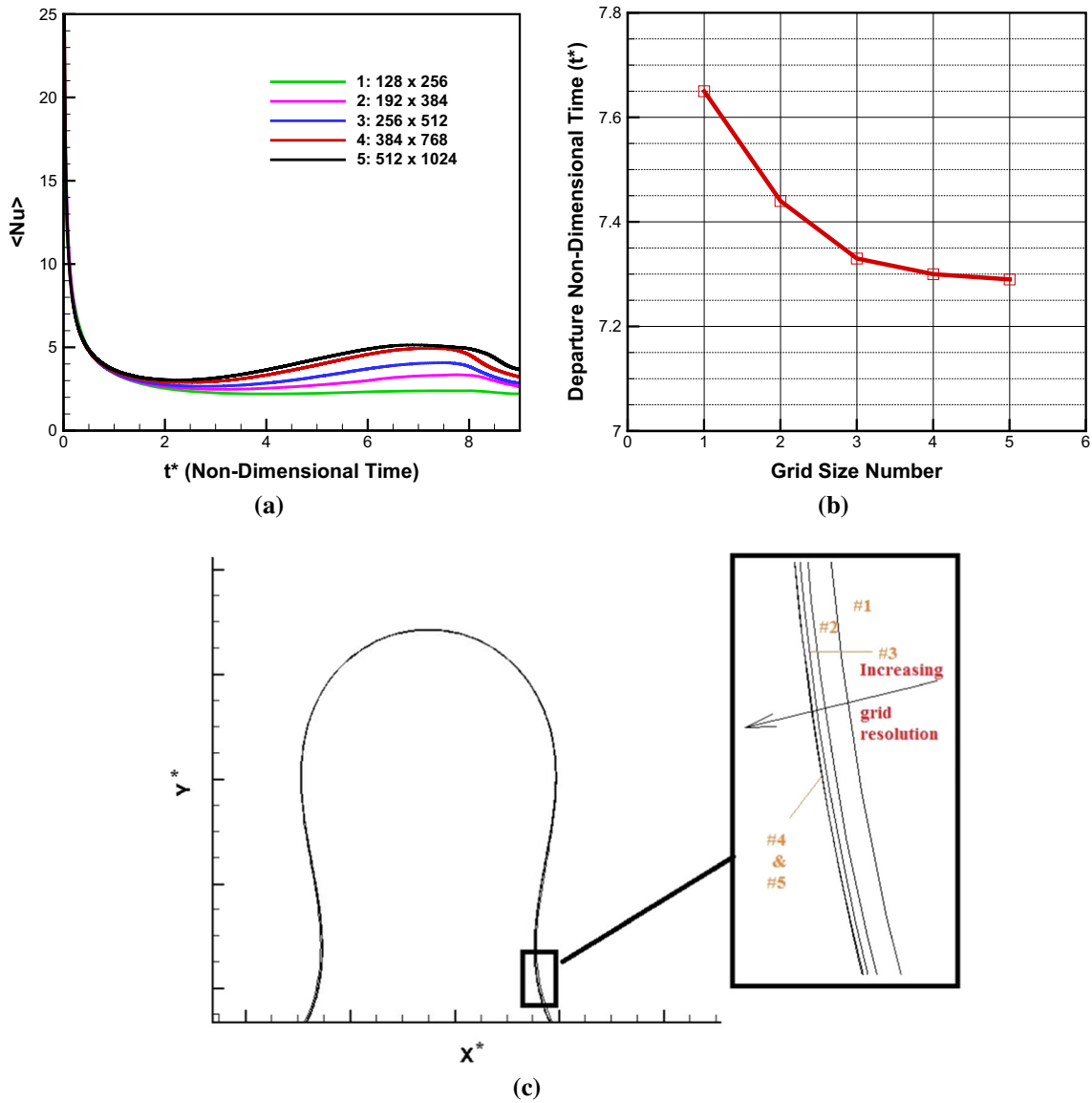
Fig. 8 Grid resolution test: **a** space-averaged Nu against non-dimensional time, **b** first bubble departure time and (c) corresponding front for different grid resolutions, the flow parameters are Pr = 4.2, Gr = 300 and Ja = 0.017

In this section, the simulations results will be validated within two different correlations presented by Sakashita and Kumada [10] and Hara [46] who considered the nucleation site density explicitly in their correlations. The main feature of the former proposed empirical correlation is that it is not limited to special working fluids and is obtained according to a few of totally different experiments using different working fluids and several combinations of boiling surfaces. The latter one is similar, but obtained analytically and examined against experimental data.

Sakashita and Kumada [10] have proposed Eq. (31) to compute the time-averaged Nusselt number using primitive physical properties in nucleate pool boiling at a wall superheat and nucleation site density and high pressures as follows:

$$\mathrm{Nu}_{\mathrm{S-K}} = 0.5 \left(\frac{\rho_1 u_0 l_0}{\mu_1} \right)^{\frac{1}{3}} \left(\frac{k_1}{\rho_1 c_1 u_0 l_0} \right)^{-\frac{1}{6}} \left(\frac{\rho_1 u_0^2 l_0}{\sigma} \right)^{-\frac{1}{4}} \Delta T^{-\frac{1}{3}} n^{\frac{3}{8}}, \tag{33}$$
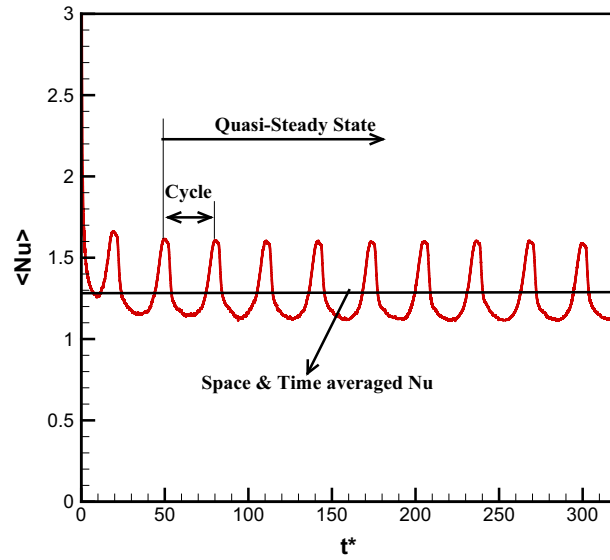
Fig. 9 Nusselt number as a function of time during 10-bubble departure from heater surface in nucleate pool boiling when Gr = 17.85, Pr = 4.2, Ja = 0.064
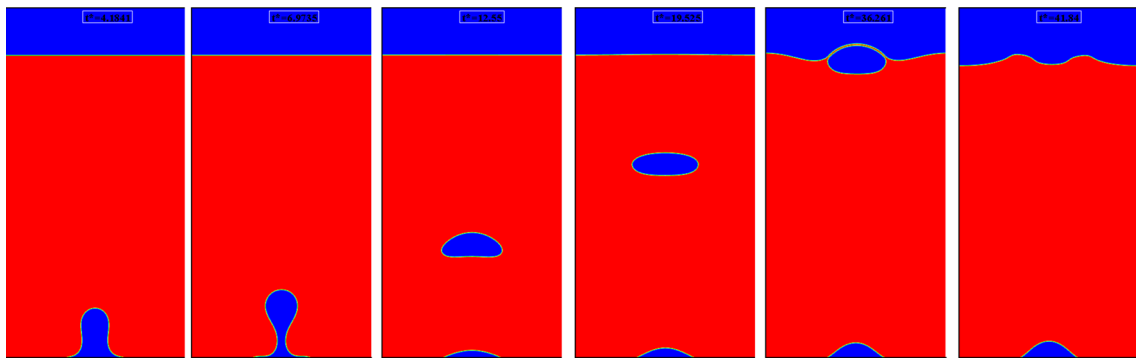

Fig. 10 The time evolution contour plots of phases field during complete cycle of nucleate pool boiling including particular instance before and after breakup of growing bubble and coalescence of rising bubble with top vapor layer where flow parameters are Gr = 150, Ja = 0.03, Pr = 4.2

where Nu_{S-K} is in fact the space- and time-averaged Nusselt number. Additionally, Eq. (31) is reported in terms of all related primitive variables including the properties of liquid and vapor phase. Hara [46] also reported another correlation which is in fairly good agreement with experimental data [17] as below:

$$Nu_H = (C_1 C_2)^{\frac{3}{4}} \left(\frac{4\pi C_2}{3} \right)^{-\frac{1}{2}} \left(\frac{k_l}{\rho_l c_l l_0} \right)^{-\frac{1}{4}} \Delta T^{\frac{1}{2}} n^{\frac{3}{8}}, \tag{34}$$

where $C_1 = 5.5$ and $C_2 = 0.056$ are the constants of the correlation. We chose the flow condition in which Gr = 150, Pr = 4.2 and Ja = 0.03 and obtained the space- and time-averaged Nusselt number for one complete cycle as $<\overline{Nu}> = 1.768$. Also, Fig. 10 shows more details regarding the time evolution contour plot of the phases field during pool boiling.

The corresponding primitive variables of the simulation were put in the correlations and the results are reported in Table 4. It is observed that, the predictions of the present study are in fairly good agreement with empirical correlation. Actually, the obtained numerical prediction falls between the corresponding results reported in Table 4. The over prediction and underestimation of the present work are + 19% and − 25%, respectively, regarding the available correlations in the literature. It should be noted that, these levels of relative errors are reasonable and well accepted in the field of boiling flow research [44].

In the following, the study focuses on effective non-dimensional parameters in nucleate pool boiling to find out how the variation of each parameter affects the heat transfer rate. Although the properties of the

Table 4 Summary of results obtained for $<\overline{Nu}>$ and comparison between present work and other experimental and analytical studies for nucleate pool boiling when Gr = 150, Pr = 4.2, Ja = 0.03

Description	Time- and space-averaged Nusselt number $<\overline{Nu}>$	Relative error %	
		Sakashita and Kumada's correlation	Hara's correlation
Present study (numerical simulation)	1.768	− 25%	+ 19%
Sakashita and Kumada [10] NuS-K	1.415	Ref. value	Not applicable
Hara [46] NuH	2.208	Not applicable	Ref. value

working fluid of the present study correspond to water at high pressures, the variation of the non-dimensional parameters removes the restriction imposed by the properties of water. Thus, the present study is not limited to a special fluid or material.

3.7 Effect of the Grash of number

The effect of the Grashof number is investigated while the Prandtl and Jacob numbers as well as the dimensionless properties are fixed. Here, the Grashof number changes in the range 17 to 300 and the space-averaged Nusselt number, i.e., $<Nu>$ and the time-averaged Nusselt number, i.e., $<\overline{Nu}>$, will be reported for different cases. The simulations are proceeded long enough so that a few complete cycles have occurred and ascertain that the initial condition and early times do not significantly affect the overall results. As is well described by Jiang et al. [47], several forces, including buoyancy, attaching surface tension, inertia due to phase change, drag and expelled liquid, simultaneously act on the growing bubble attached to the boiling surface that cause a very complex situation. Besides, the stochastic nature of the nucleation and growth process during the nucleate boiling phenomenon, has ended up most researchers to apply the overall and statistical results to ignore the detailed physics and could more simply study this process. Here, we try to depict a level of detailed physics by presenting the boiling surface space-averaged Nusselt number as a function of time along with time average results.

In order to clearly understand how the Grashof number influences nucleate pool boiling, the detailed behavior of the space-averaged Nusselt number is presented in Fig. 11a. Also, Fig. 11b shows the cycle mean time averaged as the representative of the overall behavior of the flow. Under this flow condition, increasing the Grashof number rises the time-averaged Nusselt number due to significant growth of peak value according to Fig. 11a.

Physically, the detachment of the growing bubble from the boiling surface leads to a peak in the space-averaged Nusselt number. This is due to the bubble departure from the boiling surface that enhances the convective effects. After the bubble departs from the boiling surface, a considerable amount of the saturated liquid moves toward the heated plate to fill the bubble original position. This phenomenon is well known in the literature and is termed as the rewetting being one of the sub-processes of nucleate pool boiling [4]. Except for the first bubble departure, the peak values of the space-averaged Nusselt number during the nucleate boiling process are nearly constant for a specific Grashof number. Furthermore, as it is shown in Fig. 11a the peak value severely increases as the Gr number is raised. Additionally, the departure time period, i.e., time elapsed from initial seed to departure instant, increases as well. Statistically, the number of peaks and the corresponding magnitude of each peak determine the value of the time-averaged Nusselt number. As is revealed in Fig. 11b, the overall results of these factors cause an increase in the Nusselt number when the Grashof number is raised.

The shape of the detached bubble from the surface is presented in Fig. 12 for different Grashof numbers. An increase in Grashof number leads to a rise in the magnitude of vertical velocity component and therefore a change in the shape and size of the detached bubble. Although increasing the size of the detached bubble leads to a decrease in the frequency of the bubble detachment, this will enhance the convective heat transfer effect near the boiling surface by increasing the region of the liquid displacement. Accordingly, increasing the Grashof number enhances the time-averaged heat transfer because of a significant growth of peak values observed in Fig. 11.
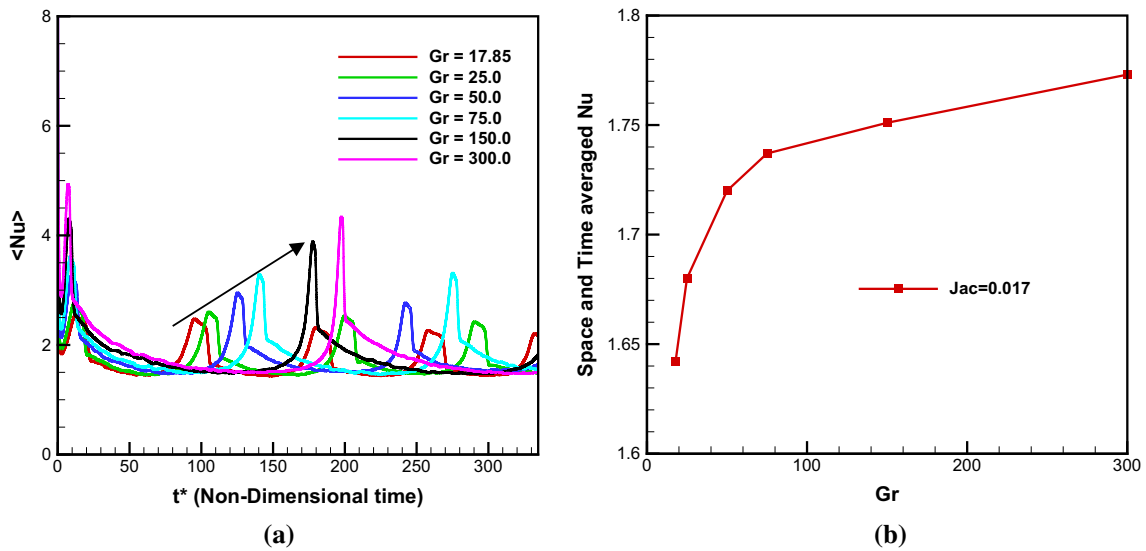
Fig. 11 Effect of Grashof number **a** on space-averaged Nu versus non-dimensional time when Ja = 0.017 and Pr = 4.2 and **b** time-averaged Nusselt number as a function of Grashof number when Ja = 0.017 and Pr = 4.2
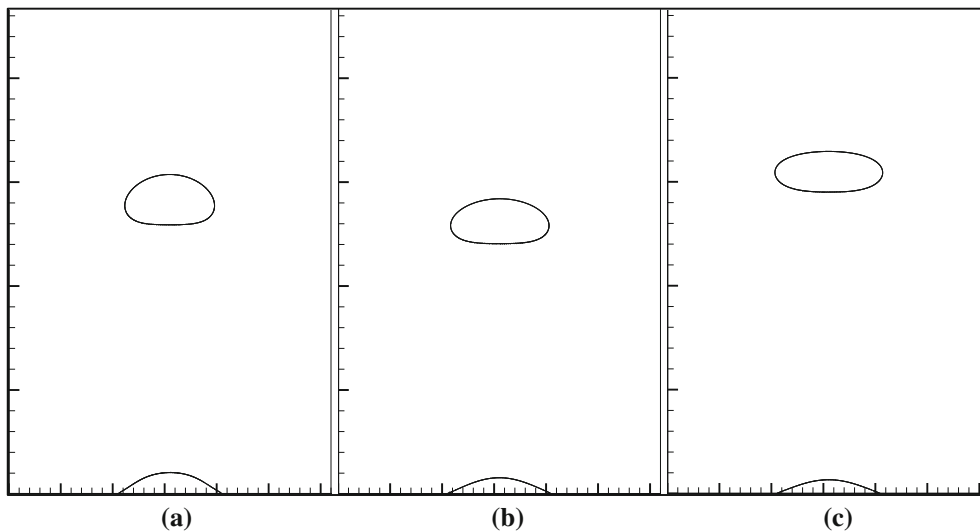

Fig. 12 Size and shape of the detached bubble right after the departure moment from the boiling surface when Pr = 4.2 and Ja = 0.017, **a** Gr = 17.78, **b** Gr = 150 and **c** Gr = 300

3.8 Effect of the Prandtl number

Here, the effect of Prandtl number is addressed while the Grashof and Jacob numbers as well as the dimensionless properties are fixed. The Prandtl number has been varied in the range of 2.8 to 8.6 and the space-averaged Nusselt number, <Nu>, and the time- and space-averaged Nu, i.e., $\overline{<Nu>}$, are reported for different cases. All the other flow parameters are the same as what has been described in the preceding section.

In order to analyze how the Prandtl number influences the nucleate pool boiling, the detailed behavior of the space-averaged Nusselt number is displayed in Fig. 13a. Also, Fig. 13b shows the mean time-averaged Nusselt number over one cycle based on the repeated numerical simulations carried out at different Grashof numbers (i.e., 17.85, 50, 150 and 300) to better realize the effect of this parameter.

As can be observed in Fig. 13a, the peaks enhance as the Prandtl number increases as well as the departure period increases. Statistically, the number of peaks and the corresponding magnitude determine the value of the time-averaged Nusselt number. Figure 13b indicates that the time-averaged Nusselt number increases when the Prandtl number is raised. At a specific Grashof number, an increase in the Prandtl number will increase
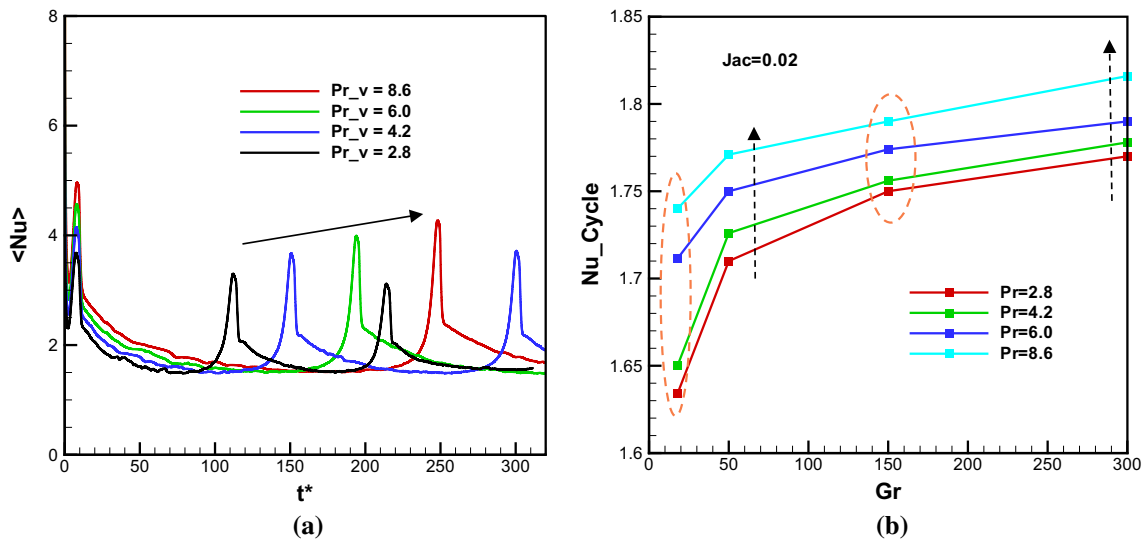
Fig. 13 Effect of Prandtl number **a** on space-averaged Nu when Gr = 150 and Ja = 0.02 and **b** time-averaged Nu as a function of Gr where Ja = 0.02

the time-averaged Nusselt number, and for a specific Prandtl number increasing the Grashof number will raise the space- and time-averaged Nusselt number. Actually, here the increase in the bubble detachment frequency with smaller bubble size during a specific time interval could not compensate the effect of dominant convective effect due to bubble displacement and rewetting that has occurred after the bubble departure with a greater size. It should be noted that for all of the conducted simulations presented in Fig. 13b, the Jacob number is fixed.

3.9 Effect of Jacob number

To evaluate the effect of Jacob number on nucleate pool boiling, some simulations with different Jacob numbers are performed while the Prandtl number as well as the Grashof number are constant. For a given ratio of the properties increasing the wall superheat leads to an increase in the Jacob number.

Here, the Jacob number has been varied in the range from 0.017 to 0.05 and the space-averaged Nusselt number, i.e., $<Nu>$ and, time and space-averaged Nu, i.e., $<\overline{Nu}>$, are reported for different cases. Physically, the value of the Jacob number should be chosen within the mentioned range due to two reasons. First, it should be large enough to make sure that nucleate pool boiling will definitely occur, and second, the nucleate pool boiling process is maintained in a regime with isolated nucleation sites. All the other considerations of the simulations are the same as what have already been presented in the preceding sections.

In order to clarify how the Jacob number affects the nucleate pool boiling, the detailed behavior of the space-averaged Nusselt numbers is shown in Fig. 14a. Additionally, Fig. 14b shows the mean time-averaged Nusselt number over one cycle as the representative of the boiling process. It also shows, the results of the repeated numerical simulations carried out at different Grashof numbers (i.e., 17.85, 50, 150 and 300) to better realize the effect of this parameter.

As is displayed in Fig. 14a, an increase in the Jacob number causes an increase in the frequency of the bubble detachment, and the peaks of the space-averaged Nusselt numbers decrease slightly. Here, the enhancement of the bubble departure frequency has occurred such that the mean time-averaged Nusselt number increases, even though the corresponding peaks have been reduced. It is also found that for a given Grashof number increasing the Jacob number always raises the time-averaged Nusselt number. Physically, it is postulated that under the considered condition the frequency of bubble detachment is dominant that controls the heat transfer rate from the boiling surface.
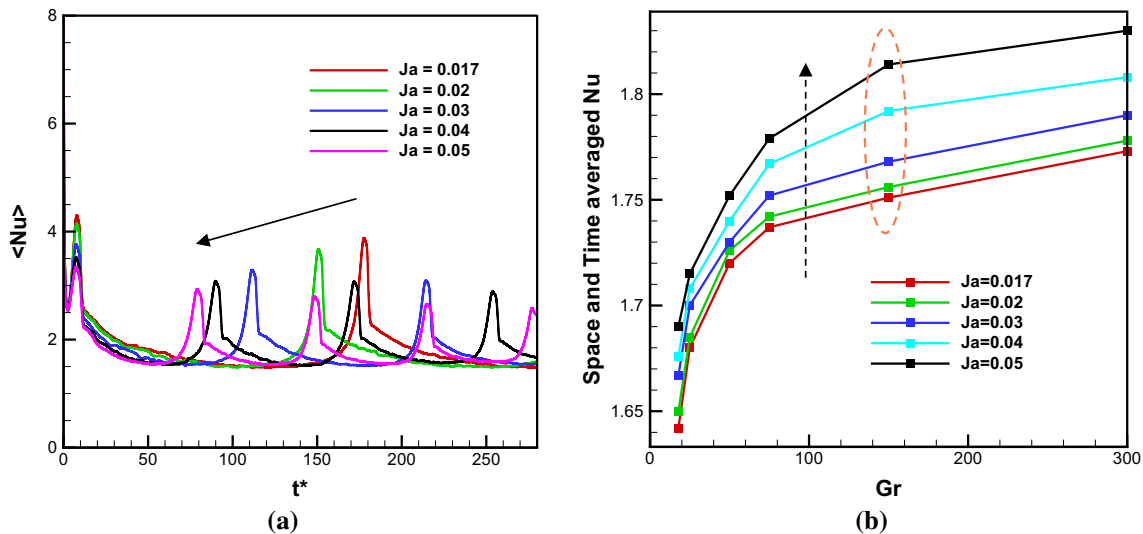
Fig. 14 Effect of Jacob number **a** on space-averaged Nusselt number as a function of t^* when Gr = 150 and Pr = 4.2 and **b** space-and time-averaged Nusselt number as a function of Grashof number when Pr = 4.2

4 Conclusions

In this paper, direct numerical simulations of saturated nucleate pool boiling process from a constant temperature boiling surface were carried out using a front tracking method. Here, the computational code has been developed to take into account the phase change along the interface and then adopted the solver to the flow and heat transfer during several sequential cycles. The present developed solver has been verified by means of different analytical, numerical and experimental standard test cases and a very good agreement was observed. Although the complete cycle of nucleate boiling including nucleation seed growth, rising and departing from the heated wall is captured, we focused on overall and average results to analyze the heat transfer rate during pool boiling. This way, effects of the main non-dimensional pertinent parameters and fluid properties variation on heat transfer from the boiling surface are investigated for a given nucleation site density within the isolated bubble region. The overall behavior of changing different dominant parameters is well reported according to results obtained for the frequency of bubble departure and the corresponding peaks of the Nusselt number, which basically depend on the bubble departure diameter. The study attempted to address the situation at high pressures where reliable experimental data are rare. Additionally, we introduced a new insight on this topic by which the analysis is not limited to some most common working fluids and special boiling surfaces. Definitely, there exists a considerable amount of work that has to be accomplished to complete the present study on the proposed approach.

References

1. Liang, G., Yu, H., Chen, L., Shen, S.: Interfacial phenomena in impact of droplet array on solid wall. Acta Mech. **231**(1), 305–319 (2020)
2. Mansour, T.M., Khalaf-Allah, R.A.: Theoretical and experimental verification for determining pool boiling heat transfer coefficient using fuzzy logic. Heat Mass Transf. **56**(11), 3059–3070 (2020)
3. Nukiyama, S.: The maximum and minimum values of the heat Q transmitted from metal to boiling water under atmospheric pressure. Int. J. Heat Mass Transf. **9**(12), 1419–1433 (1966)
4. Kim, J.: Review of nucleate pool boiling bubble heat transfer mechanisms. Int. J. Multiph. Flow **35**(12), 1067–1076 (2009)
5. Yagov, V.V.: Nucleate boiling heat transfer: possibilities and limitations of theoretical analysis. Heat Mass Transf. **45**(7), 881–892 (2009)
6. Jo, H., Ahn, H.S., Kang, S., Kim, M.H.: A study of nucleate boiling heat transfer on hydrophilic, hydrophobic and heterogeneous wetting surfaces. Int. J. Heat Mass Transf. **54**(25), 5643–5652 (2011)
7. Tien, C.: A hydrodynamic model for nucleate pool boiling. Int. J. Heat Mass Transf. **5**(6), 533–540 (1962)
8. Rohsenow, W.: A new correlation of pool-boiling data including the effect of heating surface characteristics. Stainl. Steel **1**(111), 1 (1968)
9. Kocamustafaogullari, G., Ishii, M.: Interfacial area and nucleation site density in boiling systems. Int. J. Heat Mass Transf. **26**(9), 1377–1387 (1983)

10. Sakashita, H., Kumada, T.: Method for predicting boiling curves of saturated nucleate boiling. Int. J. Heat Mass Transf. **44**(3), 673–682 (2001)
11. Danish, M., Al Mesfer, M.K.: Analytical solution of nucleate pool boiling heat transfer model based on macrolayer. Heat Mass Transf. **54**(2), 313–324 (2018)
12. Zajaczkowski, B., Halon, T., Krolicki, Z.: Experimental verification of heat transfer coefficient for nucleate boiling at sub-atmospheric pressure and small heat fluxes. Heat Mass Transf. **52**(2), 205–215 (2016)
13. Son, G., Dhir, V.: Numerical simulation of saturated film boiling on a horizontal surface. Trans. Am. Soc. Mech. Eng. J. Heat Transf. **119**, 525–533 (1997)
14. Son, G., Dhir, V.: Numerical simulation of film boiling near critical pressures with a level set method. Trans. Am. Soc. Mech. Eng. J. Heat Transf. **120**, 183–192 (1998)
15. Tryggvason, G., et al.: A front-tracking method for the computations of multiphase flow. J. Comput. Phys. **169**(2), 708–759 (2001)
16. Li, Q., Kang, Q., Francois, M.M., He, Y., Luo, K.: Lattice Boltzmann modeling of boiling heat transfer: the boiling curve and the effects of wettability. Int. J. Heat Mass Transf. **85**, 787–796 (2015)
17. Shin, S., Abdel-Khalik, S., Juric, D.: Direct three-dimensional numerical simulation of nucleate boiling using the level contour reconstruction method. Int. J. Multiph. Flow **31**(10), 1231–1242 (2005)
18. Welch, S.W.: Local simulation of two-phase flows including interface tracking with mass transfer. J. Comput. Phys. **121**(1), 142–154 (1995)
19. Ryu, S., Ko, S.: Direct numerical simulation of nucleate pool boiling using a two-dimensional lattice Boltzmann method. Nucl. Eng. Des. **248**, 248–262 (2012)
20. Mohammadpourfard, M., Aminfar, H., Sahraro, M.: Numerical simulation of nucleate pool boiling on the horizontal surface for ferrofluid under the effect of non-uniform magnetic field. Heat Mass Transf. **50**(8), 1167–1176 (2014)
21. Sato, Y., Niceno, B.: A depletable micro-layer model for nucleate pool boiling. J. Comput. Phys. **300**, 20–52 (2015)
22. Sato, Y., Niceno, B.: Nucleate pool boiling simulations using the interface tracking method: boiling regime from discrete bubble to vapor mushroom region. Int. J. Heat Mass Transf. **105**, 505–524 (2017)
23. Sato, Y., Niceno, B.: Pool boiling simulation using an interface tracking method: from nucleate boiling to film boiling regime through critical heat flux. Int. J. Heat Mass Transf. **125**, 876–890 (2018)
24. Murallidharan, J., Giustini, G., Sato, Y., Ničeno, B., Badalassi, V., Walker, S.P.: Computational fluid dynamic simulation of single bubble growth under high-pressure pool boiling conditions. Nucl. Eng. Technol. **48**(4), 859–869 (2016)
25. Yazdani, M., Radcliff, T., Soteriou, M., Alahyari, A.A.: A high-fidelity approach towards simulation of pool boiling. Phys. Fluids **28**(1), 012111 (2016)
26. Esmaeeli, A., Tryggvason, G.: Computations of film boiling. Part I: numerical method. Int. J. Heat Mass Transf. **47**(25), 5451–5461 (2004)
27. Razavieh, A., Mortazavi, S.: The interface between fluid-like and solid-like behavior for drops suspended in two-phase Couette flow. Acta Mech. **226**(4), 1105–1121 (2015)
28. Khalili, H., Mortazavi, S.: Numerical simulation of buoyant drops suspended in Poiseuille flow at nonzero Reynolds numbers. Acta Mech. **224**(2), 269–286 (2013)
29. Peskin, C.S.: Numerical analysis of blood flow in the heart. J. Comput Phys. **25**(3), 220–252 (1977)
30. Schumann, U., Sweet, R.A.: A direct method for the solution of Poisson's equation with Neumann boundary conditions on a staggered grid of arbitrary size. J. Comput. Phys. **20**(2), 171–182 (1976)
31. Udaykumar, H., Shyy, W., Rao, M.: ELAFINT-A mixed Eulerian-Lagrangian method for fluid flows with complex and moving boundaries. In: 6th joint thermophysics and heat transfer conference, pp. 1996 (1996)
32. Juric, D., Tryggvason, G.: Computations of boiling flows. Int. J. Multiph. Flow **24**(3), 387–410 (1998)
33. Welch, S.W.J., Wilson, J.: A Volume of fluid based method for fluid flows with phase change. J. Comput. Phys. **160**(2), 662–682 (2000)
34. Esmaeeli, A., Tryggvason, G.: Computations of explosive boiling in microgravity. J. Sci. Comput. J. Artic. **19**(1), 163–182 (2003)
35. Irfan, M., Muradoglu, M.: A front tracking method for direct numerical simulation of evaporation process in a multiphase system. J. Comput. Phys. **337**, 132–153 (2017)
36. Esmaeeli, A., Tryggvason, G.: Computations of film boiling. Part II: multi-mode film boiling. Int. J. Heat Mass Transf. **47**(25), 5463–5476 (2004)
37. Berenson, P.J.: Film-boiling heat transfer from a horizontal surface. J. Heat Transf. **83**(3), 351–356 (1961)
38. Klimenko, V.V., Shelepen, A.G.: Film boiling on a horizontal plate—a supplementary communication. Int. J. Heat Mass Transf. **25**(10), 1611–1613 (1982)
39. Muradoglu, M., Romanò, F., Fujioka, H., Grotberg, J.B.: Effects of surfactant on propagation and rupture of a liquid plug in a tube. J. Fluid Mech. **872**, 407–437 (2019)
40. Esmaeeli, A., Tryggvason, G.: A front tracking method for computations of boiling in complex geometries. Int. J. Multiph. Flow **30**(7), 1037–1050 (2004)
41. Razizadeh, M., Mortazavi, S., Shahin, H.: Drop breakup and drop pair coalescence using front-tracking method in three dimensions. Acta Mechanica, journal article **229**(3), 1021–1043 (2018)
42. Pioro, I.L., Rohsenow, W., Doerffer, S.S.: Nucleate pool-boiling heat transfer. I: review of parametric effects of boiling surface. Int. J. Heat Mass Transf. **47**(23), 5033–5044 (2004)
43. Sakashita, H.: Bubble growth rates and nucleation site densities in saturated pool boiling of water at high pressures. J. Nucl. Sci. Technol. **48**(5), 734–743 (2011)
44. Pioro, I.L., Rohsenow, W., Doerffer, S.S.: Nucleate pool-boiling heat transfer. II: assessment of prediction methods. Int. J. Heat Mass Transf. **47**(23), 5045–5057 (2004)
45. Dhir, V. K., Warrier, G. R., Aktinol, E.: Numerical simulation of pool boiling: a review. J. Heat Transf. 135(6), 061502 (2013)
46. Hara, T.: The mechanism of nucleate boiling heat transfer. Int. J. Heat Mass Transf. **6**(11), 1–17 (1963)

47. Jiang, Y.Y., Osada, H., Inagaki, M., Horinouchi, N.: Dynamic modeling on bubble growth, detachment and heat transfer for hybrid-scheme computations of nucleate boiling. Int. J. Heat Mass Transf. **56**(1), 640–652 (2013)